Title

Contribution of biomimetic collagen-ligand interaction to intrafibrillar mineralization

Journal

Science Advances, 5(3)

ISSN

2375-2548

Authors

Song, Q
Jiao, K
Tonggu, L
et al.

Publication Date

2019-03-01

DOI

10.1126/sciadv.aav9075

MATERIALS SCIENCE

Contribution of biomimetic collagen-ligand interaction to intrafibrillar mineralization

Q. Song[1]*, K. Jiao[1]*, L. Tonggu[2], L. G. Wang[2], S. L. Zhang[3], Y. D. Yang[4], L. Zhang[3], J. H. Bian[4], D. X. Hao[3], C. Y. Wang[1], Y. X. Ma[1], D. D. Arola[5], L. Breschi[6], J. H. Chen[1†], F. R. Tay[1,7†], L. N. Niu[1†]

Contemporary models of intrafibrillar mineralization mechanisms are established using collagen fibrils as templates without considering the contribution from collagen-bound apatite nucleation inhibitors. However, collagen matrices destined for mineralization in vertebrates contain bound matrix proteins for intrafibrillar mineralization. Negatively charged, high–molecular weight polycarboxylic acid is cross-linked to reconstituted collagen to create a model for examining the contribution of collagen-ligand interaction to intrafibrillar mineralization. Cryogenic electron microscopy and molecular dynamics simulation show that, after cross-linking to collagen, the bound polyelectrolyte caches prenucleation cluster singlets into chain-like aggregates along the fibrillar surface to increase the pool of mineralization precursors available for intrafibrillar mineralization. Higher-quality mineralized scaffolds with better biomechanical properties are achieved compared with mineralization of unmodified scaffolds in polyelectrolyte-stabilized mineralization solution. Collagen-ligand interaction provides insights on the genesis of heterogeneously mineralized tissues and the potential causes of ectopic calcification in nonmineralized body tissues.

INTRODUCTION

Biomineralization is a process in which inorganic elements are selectively deposited on specific organic macromolecules under the precise control of organisms to produce biological minerals. On the basis of the inorganic species present, biomineralization may be divided into biocalcification and biosilicification, in which collagen is used as a universal template (*1*). More than half of the biominerals in nature are calcium-containing minerals, such as calcium phosphate (CaP) and octacalcium phosphate. CaP-containing biominerals constitute the hard connective tissues of vertebrates, whereas calcium carbonate forms the skeleton of invertebrates. Because the concept of biocalcification has been gradually replaced by biomineralization, we used the term "mineralization" in this work to refer to the deposition of CaP within an organic template. The use of collagen fibrils as mineralization templates is appealing because the nanoscopical channels present within these fibrillar structures enable ordered deposition of mineral platelets to produce nanoengineered hybrid materials with combined strength and resilience (*2*). Intrafibrillar mineralization cannot be achieved by simply immersing collagen matrices in a supersaturated solution of mineral ions and requires the use of nucleation inhibitors to stabilize the ion association complexes and prevent them from crystallizing outside the fibrils (*3*). Over the last decade, different in vitro models have been proposed for understanding the mechanisms of intrafibrillar mineralization (*4*). These models capitalize on the classical ion cluster–based and the nonclassical particle-based crystallization pathways for explaining how mineralization precursors infiltrate the intrafibrillar water compartments of collagen fibrils (*5*). Models based on the classical theory of crystallization include electrostatic attraction of ion clusters along the e-band of collagen fibrils (*6*), prevention of nucleation inhibitors from entering the collagen fibrils based on their size exclusion characteristics (*7*), and precipitation of intrafibrillar mineral platelets from ion clusters during self-assembly of the collagen fibrils (*8*). Models based on the nonclassical theory of crystallization include capillary imbibition of polymer-stabilized, liquid amorphous mineralization precursors (*9*); electrostatic attraction of negatively charged prenucleation clusters to the positively charged a-band of collagen fibrils (*10*); and simultaneous establishment of osmotic equilibrium and electroneutrality along the surface of collagen fibrils with semipermeable characteristics (*11*). In all these models, the inhibitors for delaying crystal nucleation are incorporated in the mineralization medium and are not bound to the collagen fibrils. Such a scenario does not represent what occurs in biological systems.

It is known that macromolecules present in the extracellular matrix have to bind to collagen fibrils for optimal functioning. Protein ligands such as integrins, kinases, fibronectin, and matrix metalloproteinases have three-dimensional (3D) configurations within which discrete collagen-binding domains are present for binding to collagen (*12*). Matrix proteins involved in biomineralization are no exception; even before the advent of various in vitro intrafibrillar mineralization models, specific collagen binding sites have been reported in noncollagenous proteins (*13*). Osteocalcin, one of the most abundant noncollagenous proteins in bone, has been detected in both the gap zone and the overlap zone of collagen fibrils and appear as single spheres or pearl necklace–like strings (*14*, *15*). Guanidine and collagenase extraction studies demonstrated that matrix phosphoproteins bind to collagen via ion association or covalent bonding (*16*). Collagen secreted by fibroblasts does not mineralize in the presence of mineralization precursors except for areas with ectopic calcification

[1]State Key Laboratory of Military Stomatology & National Clinical Research Center for Oral Diseases & Shaanxi Key Laboratory of Stomatology, School of Stomatology, The Fourth Military Medical University, Xi' an, Shaanxi, PR China. [2]Department of Biological Structure, School of Medicine, University of Washington, Seattle, WA, USA. [3]Department of Applied Physics, Xi'an Jiaotong University, Xi'an, Shaanxi, PR China. [4]Frontier Institute of Science and Technology and State Key Laboratory for Mechanical Behavior of Materials, Xi'an Jiaotong University, Xi'an, Shaanxi, PR China. [5]Department of Materials Science & Engineering, University of Washington, Seattle, WA, USA. [6]Department of Biomedical and Neuromotor Sciences (DIBINEM), University of Bologna, Bologna, Italy. [7]College of Dental Medicine, Augusta University, Augusta, GA, USA.
*These authors contributed equally to this work.
†Corresponding author. Email: jhchen@fmmu.edu.cn (J.H.C.); ftay@augusta.edu (F.R.T.); niulina831013@126.com (L.N.N.)

(*17*); matrix phosphoproteins are also involved in ectopic mineralization of vascular tissues (*18*). Mineral induction with collagen-bound matrix phosphoproteins is different from what is achieved using bare collagen alone (*19*). Contemporary in vitro mineralization models are incapable of explaining why site specificity exists in different parts of the turkey leg tendon where some parts are never mineralized (*20*). These unexplained issues are examples of the knowledge gap that exists in how intrafibrillar mineralization is affected by collagen-bound nucleation inhibitors. Accordingly, the present work attempts to identify the contribution of collagen-ligand interaction to intrafibrillar mineralization and to examine whether some of the contemporary models of collagen intrafibrillar mineralization are adept at elucidating what occurs when nucleation inhibitors are bound to collagen.

Difficulty in extraction and the complicated function of physiological noncollagenous proteins limit their utilization in biomimetic mineralization. Because anionic polyelectrolytes are capable of mimicking the highly anionic, intrinsically disordered protein confirmation, high charged amino acid content, and high sequence redundancy properties that are found in noncollagenous proteins, the authors resorted to using polyelectrolytes as nucleation inhibitors for binding to matrix protein–free reconstituted collagen as models for intrafibrillar mineralization. Molecular dynamics simulation shows that a polyelectrolyte such as polyacrylic acid (PAA) is capable of caching calcium and hydrogen phosphate ion complexes into chain-like aggregates along the surface of the macromolecule when it is introduced into a supersaturated CaP mineralization medium (fig. S2). On the basis of the results of the molecular dynamics simulation, we developed a testing hypothesis that a polyelectrolyte nucleation inhibitor that is bound exclusively to the surface of collagen fibrils is capable of stabilizing CaP mineralization precursors in the vicinity of the fibrils, as well as concentrating the precursors for more efficacious intrafibrillar mineralization. We tested this hypothesis by comparison with controls in which an unbound version of the same polyelectrolytes was incorporated in the mineralization medium used for stabilizing amorphous CaP precursors.

RESULTS AND DISCUSSION

Development and characterization of nucleation inhibitor–bound collagen model

A high–molecular weight PAA (HPAA; 450 kDa) was used to simulate osteopontin, a phosphoprotein with molecular mass larger than 40 kDa (*21*), which, according to the size exclusion theory (*7*), is localized exclusively on the surface of collagen fibrils. A low–molecular weight PAA (LPAA; 2 kDa) was used to simulate osteocalcin, a phosphoprotein with molecular mass smaller than 6 kDa (*22*), which, because of its small molecular mass, can access all water compartments within a collagen fibril. These polyanionic electrolytes were chemically cross-linked to reconstituted type I collagen fibrils or sponges using carbodiimide and *N*-hydroxysulfosuccinimide. When examined by Fourier transform infrared spectroscopy (FTIR), nucleation inhibitor–bound collagen had augmented amide I, II, and III peaks compared with bare collagen (Fig. 1A), which were attributed to increases in amide linkages after cross-linking (*23*). Collagen matrices with bound PAA demonstrated marked increases in negative surface ζ potential (Fig. 1B) and carboxyl groups (Fig. 1C). Decreases in amine groups (Fig. 1D) were caused by the formation of O═C...N─H linkages. Transmission electron microscopy (TEM) of reconstituted PAA-bound collagen (PAA-collagen) fibrils stained with ruthenium red, a cationic dye, showed that the bound PAA appeared as electron-dense filamentous aggregates on the fibril surface that obscured the banding patterns of bare collagen fibrils (fig. S3). We examined the binding/release characteristics of PAA-collagen sponges using high-performance liquid chromatography. Milli-Q water used for storing PAA-collagen sponges did not contain traceable amounts of polyelectrolyte after 1 month of immersion (fig. S4A). Likewise, we did not detect PAA after extraction with 4 M guanidine HCl (fig. S4B). By contrast, PAA was detected after the PAA-collagen sponges were treated with bacterial collagenase (0.1 mg/ml) (fig. S4C). The results indicate that PAA binds tightly to type I collagen via covalent cross-linking and that the ability of PAA-collagen to stabilize CaP solution in the vicinity of collagen fibrils is not caused by PAA dissociation. Dynamic light scattering indicated that PAA-collagen was capable of stabilizing CaP mineralization precursors within 5 days, without obsessive precipitation, to provide adequate amorphous mineral phases for intrafibrillar infiltration. Nevertheless, the mineralization media stabilized by collagen-bound PAA were not as stable as the CaP solutions that were stabilized by HPAA (fig. S5).

Intrafibrillar mineralization induced by nucleation inhibitor–bound collagen

Formation of nucleation inhibitor–stabilized amorphous liquid droplets from CaP solution is an example of liquid-liquid phase separation that occurs in biological systems (*24*). CaP prenucleation clusters represent the smallest negatively charged, hydrated particulate entities (*25*) identifiable with cryogenic electron microscopy (cryo-EM) (*26*). Whereas the outcome of intrafibrillar mineralization is readily identifiable by conventional TEM, hydrated prenucleation clusters are modified after desiccation, and their involvement in the early stage of mineralization is unlikely to be accurately depicted. Hence, we used cryo-EM to identify how nucleation inhibitor–bound collagen influences the distribution of CaP mineralization precursors. When Au grids with holey carbon films were dipped into freshly prepared HPAA-stabilized CaP (HPAA-CaP) solution and vitrified, CaP prenucleation cluster singlets, in the form of discrete electron-dense spheres, and larger amorphous CaP droplets were randomly distributed within the frozen medium (Fig. 2A). Control bare collagen fibrils immersed in HPAA-CaP solution (ζ potential: −19.9 ± 2.11 eV) for 1 hour before vitrification were not yet mineralized. Prenucleation cluster singlets did not appear to be concentrated along the fibril surface; the density of these species in the vicinity of the fibril was similar to what was observed in other parts of the frozen medium. Larger amorphous CaP droplets appeared to be attached to the surface of the fibrils (Fig. 2B). Collagen fibrils cross-linked with HPAA and mineralized in unstabilized CaP solution (ζ potential: −0.88 ± 0.07 eV) for 1 to 72 hours showed assembly of chain-like prenucleation cluster aggregates on the surface of unmineralized, partially mineralized, and fully mineralized fibrils (Fig. 2, C to G). Although prenucleation cluster singlets and amorphous CaP droplets were present, they did not appear to be closely associated with the collagen surface. Movies created from electron tomography of the different phases of intrafibrillar mineralization of HPAA-bound collagen (HPAA-collagen) sponges and the corresponding *Z* projections are shown in fig. S6 and movies S2 to S4. 3D renderings of the early-phase (accumulation of prenucleation cluster aggregates around unmineralized collagen fibril), mid-phase

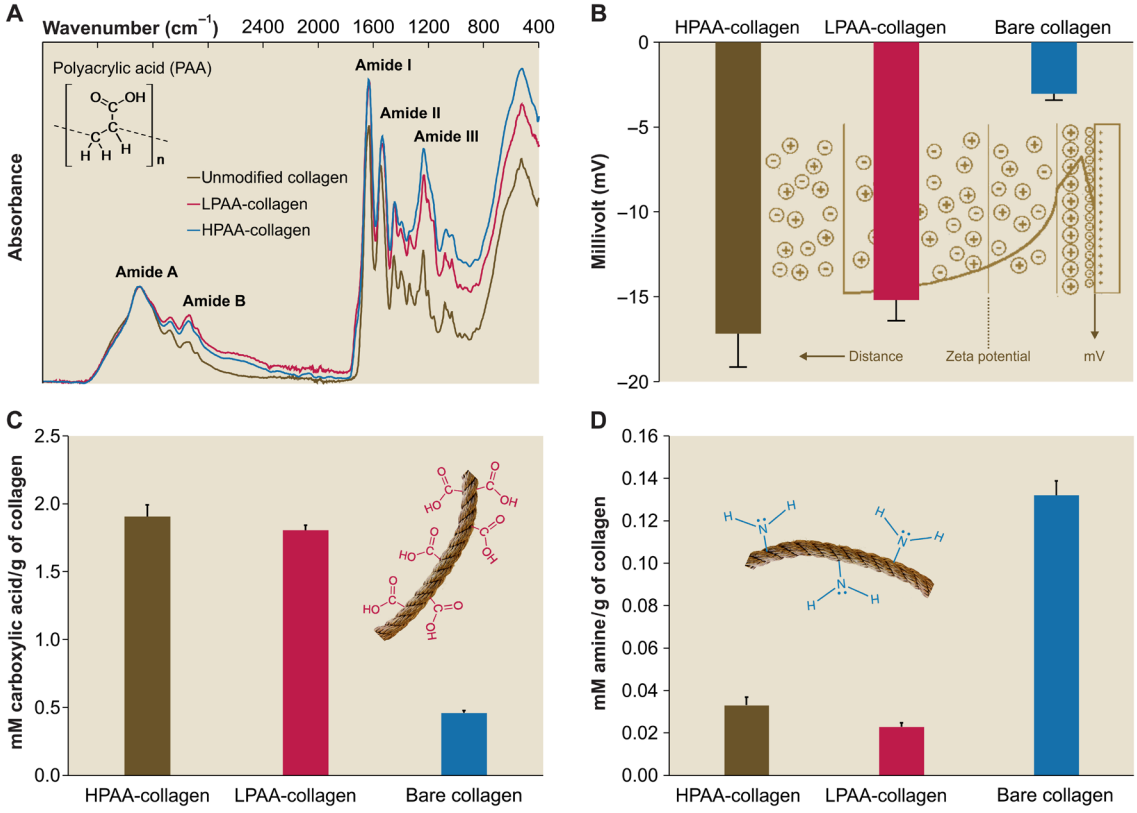

Fig. 1. Characterization of PAA-collagen. (**A**) Infrared spectra of PAA-collagen sponges. Spectra were normalized along the collagen amide A peak (~3300 cm^{-1}, NH stretch coupled with hydrogen bond). Peaks at ~1640, ~1545, and ~1240 cm^{-1} are assigned to the amide I (C═O stretch), amide II (NH bend coupled with CN stretch), and amide III (NH bend coupled with CN stretch) peaks of collagen, respectively. Peaks at ~2920 cm^{-1} are assigned to amide B (CH_2 asymmetrical stretch) bands. Compared to the spectrum of bare collagen, the spectra of HPAA-bound collagen (HPAA-collagen) and LPAA-bound collagen (LPAA-collagen) sponges show increases in the amide B, I, II, and III peaks. (**B**) Solid surface ζ potential of HPAA-collagen, LPAA-collagen, and bare collagen. Cross-linking of PAA to the collagen molecule resulted in significantly lower ζ potentials of −17.17 ± 1.98 mV for HPAA-collagen, −15.19 ± 1.22 mV for LPAA-collagen, and −3.04 ± 0.37 mV for bare collagen ($P < 0.05$ for all pairwise comparisons). (**C** and **D**) Comparison of carboxyl (C) and amine groups (D) between PAA-collagen and bare collagen. After anionic modification, the quantities of carboxyl group (in mM/g of collagen) in the HPAA-collagen (1.907 ± 0.084) and LPAA-collagen (1.807 ± 0.035) were significantly higher than that of the bare collagen (0.460 ± 0.017) because of the introduction of additional carboxyl groups to the collagen molecules ($P < 0.05$). The quantities of amine group in the HPAA-collagen (0.033 ± 0.004) and LPAA-collagen (0.023 ± 0.002) were significantly lower than that of the bare collagen (0.132 ± 0.007) because of the conjugation of free amine groups with PAA via the O═C...N−H linkage ($P < 0.05$).

(partial intrafibrillar mineralization), and late-phase (heavy intrafibrillar mineralization) mineralization of HPAA-collagen fibrils are depicted in Fig. 2 (H to J).

Compared with HPAA, LPAA-bound collagen (LPAA-collagen) sponge–stabilized amorphous CaP phases did not induce intrafibrillar mineralization of reconstituted collagen fibrils (fig. S7). Hence, LPAA was not used for subsequent experiments. With an average molecular mass of 2 kDa, LPAA enters all the water compartments of a collagen fibril; binding of LPAA to collagen is likely to be both extrafibrillar and intrafibrillar in nature. Unlike HPAA that is too large to diffuse into the intrafibrillar milieu, binding of LPAA to collagen does not satisfy the requirement for balancing osmotic equilibrium and electroneutrality simultaneously across a semipermeable membrane (*11*). Hence, establishment of Donnan equilibrium as a prerequisite for intrafibrillar mineralization mechanism is also applicable for the infiltration of unstabilized CaP into HPAA-collagen.

Attachment of the negatively charged, unstabilized CaP precursors (ζ potential: −0.88 ± 0.07 eV) to HPAA-collagen (solid ζ potential: −17.17 ± 1.98 eV) cannot be explained by electrostatic attraction. Assembly of similarly charged prenucleation cluster singlets into chain-like aggregates, without the singlets repelling each other, appears to be counterintuitive on the basis of Coulombic interpretations. Nevertheless, similar paradoxical complexations have been reported between polyelectrolytes and proteins that bear net charges of the same sign. These complexations are justified by the existence of "charged patches" on the particulate surface that enables a polyelectrolyte to bind to oppositely heterogeneous charged regions of the particulate (*27*) or by proton fluctuations caused by perturbations of acid-base equilibrium that result in regulation of the charged groups (*28*). These interactions may have accounted for the ability of collagen-bound HPAA to stabilize multiple prenucleation cluster singlets along its surface-oriented polymer chain.

Molecular dynamics simulation of the mineralization process

We validated the ability of surface-oriented collagen-bound HPAA to cache CaP mineralization precursors for intrafibrillar mineralization

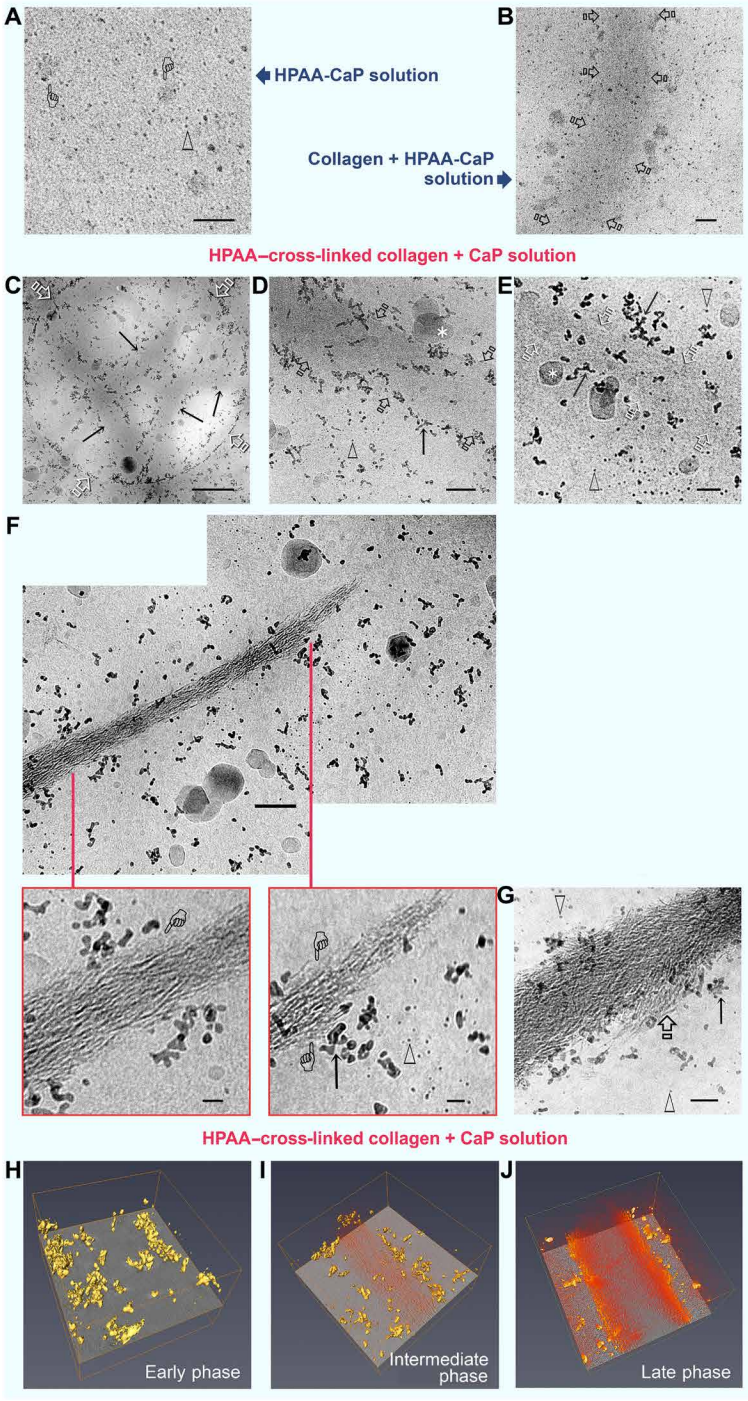

Fig. 2. Cryo-EM of mineralization of bare collagen and HPAA-collagen fibrils. (**A**) Grid dipped in freshly prepared HPAA-CaP solution. Scale bar, 50 nm. Prenucleation clusters (open arrowheads) and amorphous calcium phosphate (ACP) droplets (pointers) were randomly distributed within the frozen medium. (**B**) Grid with bare collagen immersed in HPAA-CaP for 1 hour. Scale bar, 50 nm. Fibrils (open arrows) were not mineralized at this stage. (**C** to **G**) HPAA-collagen fibrils were mineralized in unstabilized CaP solution for 1 (C and D), 8 (E), 24 (F), and 72 hours (G). Arrows, prenucleation cluster aggregates; open arrowheads, prenucleation cluster singlets; asterisks, irregular ACP droplets. (C) Circular hole in carbon film (open arrows) shows the concentration of mineral precursors along the periphery of unstained collagen fibrils (arrows). Scale bar, 500 nm. (D) Prenucleation cluster aggregates along the fibril's surface (arrows) at 1 hour. Scale bar, 100 nm. (E) At 8 hours, fibrils (open arrows) were filled with a slightly more electron-dense material. Scale bar, 50 nm. Prenucleation cluster aggregates were seen in the fibril's vicinity, while singlets were predominantly located further away. (F) Upper montage of an incompletely mineralized collagen fibril at 24 hours. Scale bar, 100 nm. Bottom left: The intrafibrillar minerals depicted by the pointer [similar to those in (E)] probably represent intrafibrillar ACP that had not yet been transformed into crystalline CaP. Scale bar, 20 nm. Bottom right: Less mineralized part of the fibril with more potentially ACP phases (pointers). Scale bar, 20 nm. (G) Heavily mineralized fibril at 72 hours shows commencement of extrafibrillar mineralization (open arrow). Scale bar, 50 nm. (**H** to **J**) 3D rendering of the early (H), middle (I), and late (J) phases of intrafibrillar mineralization of HPAA-collagen showing accumulation of prenucleation cluster aggregates (yellow) along the fibril surface; intrafibrillar minerals are depicted in orange.

via molecular dynamics simulation, using a full atomistic model of hydrated HPAA-collagen fibril complex. The collagen model was based on human FASTA protein sequence of the α1(I) and α2(I) chain components of tropocollagen (*29*). A single-unit model of collagen triple helical structures containing water molecules in the intrafibrillar regions is depicted in Fig. 3 (A and B). To investigate the effect of HPAA-collagen on ion transport from the extrafibrillar into the intrafibrillar milieu, we constructed an HPAA-collagen model by binding HPAA molecules to Lys^{1099} (1099th amino acid lysine from the N terminus) in the outmost layer of collagen microfibrils. An extended view of this model with multiple intrafibrillar and extrafibrillar units is shown in fig. S8, with the Ca^{2+}, HPO_4^{2-}, Na^+, and Cl^- ions at their ab initio states. A more detailed representation of a unit model with preestablished peripheral boundaries that was retrieved after 80 ns of simulation is illustrated in Fig. 3 (C and D). In this unit model, Ca^{2+} and HPO_4^{2-} ions, as well as assembled CaP mineralization precursors, were formed around the collagen-bound HPAA. Some of these entities could also be identified within the intrafibrillar compartment; their presence may be ascribed to Donnan equilibrium generated by the HPAA polyelectrolyte in the extrafibrillar environment (*11*). To validate this issue, we performed molecular dynamics simulation of the changes in ionic concentrations in the intrafibrillar region at designated simulation time points. Figure 3E reveals the distribution of Na^+, Cl^-, Ca^{2+}, and HPO_4^{2-} ions in the intrafibrillar and extrafibrillar regions along the axis boundary of the unit model. the decrease in the number of Na^+ and Cl^- ions within the collagen microfibrils is indicative of migration of these ions into the extrafibrillar region to balance osmotic equilibrium and electroneutrality. Concomitantly, the number of Ca^{2+} and HPO_4^{2-} ions in the intrafibrillar region increased with simulation time. Under the same ionic concentrations, the intrafibrillar infiltration of CaP precursors was comparatively sparser in the control, in which unbound HPAA was present in the vicinity of the collagen microfibrillar structures (Fig. 3F). When the intrafibrillar distributions of Na^+, Cl^-, Ca^{2+}, and HPO_4^{2-} ions in the HPAA-collagen model and the bare collagen model were compared, more intrafibrillar Ca^{2+} and HPO_4^{2-} were present in the former model (Fig. 3G).

We examined structural variations of the collagen molecules to identify changes in the intrafibrillar environment as a result of the establishment of Donnan equilibrium. The root mean square deviations of the collagen backbones increased with simulation time in both the HPAA-collagen and the bare collagen systems (Fig. 3H). This observation infers contraction of the collagen molecules for both systems to generate the osmotically driven intrafibrillar stresses for infiltration of CaP precursors (*30*). In the HPAA-collagen model, the solvent-accessible surface area (SASA) of the collagen molecules decreased from 607,141.43 to 602,944.08 Å (0.69%) over a period of 80 ns (Fig. 3I). By contrast, the SASA of collagen molecules in the unbound HPAA model decreased from 602,611.13 to 599,438.37 Å (0.53%). These results are attributed to diffusion of ions and water molecules out of the intrafibrillar water compartments into the extrafibrillar region as the free and loosely bound water is replaced by minerals.

Comparison between the collagen mineralized with two different schemes

Ultrastructural examination is incapable of truly discerning the differences in the quality of intrafibrillar mineralization achieved by bare collagen mineralized in HPAA-CaP and HPAA-collagen mineralized in unstabilized CaP. These issues are resolved by testing of mechanical properties using nanoindentation of single-collagen fibrils and compressive testing of collagen sponges. We examined the Young's moduli of unmineralized and mineralized collagen fibrils in the lengthwise and transverse directions using atomic force microscopy (AFM) operated in the bimodal amplitude–frequency modulation imaging mode. Representative amplitude and Young's modulus mappings of carbodiimide–cross-linked bare collagen before (BC) and after immersion in CaP (BC + CaP) or HPAA-CaP (BC + HPAA-CaP) and HPAA-collagen after immersion in unstabilized CaP solution (HPAA-Col + CaP) are shown in Fig. 4, respectively. The lengthwise and transverse moduli of the four groups were, in ascending order, BC < BC + CaP < BC + HPAA-CaP < HPAA-Col + CaP [analysis of variance (ANOVA) and post hoc pairwise comparisons, $P < 0.05$]. The values are similar to previously reported values for unmineralized and mineralized fibrils obtained by nanoindentation methods (*31*). Before mineralization, bare collagen exhibited sinusoidal variations in its lengthwise Young's modulus that reflect differences in tropocollagen density (*32*) and differences in shrinkage that echo variations in free water between the gap and overlap regions along the fibril's longitudinal axis (*33*). Fluctuations in Young's modulus were irregular after the bare fibrils were immersed in unstabilized CaP because of the precipitation of extrafibrillar crystallites on the surface of fibrils with minimal intrafibrillar mineralization. In comparison, periodic variations were weak and low in amplitude in the two intrafibrillar-mineralized fibril groups because of the filling of the gap zones and microfibrillar spaces with apatite nanoplatelets, as well as progressive depletion of the compartmentalized free water during intrafibrillar mineralization (*34*). X-ray diffraction indicated that the minerals present in both types of mineralized sponges were apatite (fig. S9A).

Because of their 3D nature, collagen sponges have characterization opportunities not achievable using single-layer collagen. The results of thermogravimetric analysis showed that HPAA-collagen mineralized in CaP solution for 7 days yielded higher mineral content (77.03%) than that of the bare collagen mineralized in HPAA-CaP solution (66.07%) (fig. S9B). This may be attributed to the more consistent intrafibrillar mineralization of the center of the leaflets in the HPAA-Col + CaP group (Fig. 5, A and B). We monitored the progress of mineralization in the two types of mineralized sponges with dynamic FTIR over 7 days (Fig. 5, C and E, and fig. S9C). Analysis of the apatite/collagen ratio in those spectroscopical profiles indicated that HPAA-collagen sponges were more heavily mineralized at any time point over the entire period (Fig. 5D). Stress-strain responses performed by uniaxial compression testing of the two types of mineralized sponges indicated that the tangent moduli of the two mineralized matrices were not significantly different at 0 to 5% strain (Student's *t* test, $P > 0.05$; Fig. 5, F and G); below the proportional limit, the tangent modulus is equivalent to the Young's modulus. However, the modulus of toughness, which represents the energy per unit volume that a material can absorb before rupturing, was more consistent and significantly higher for the HPAA-collagen sponges (Student's *t* test, $P < 0.05$; Fig. 5, F and G). Such a feature, which accounts for the increased resilience and high work of fracture of biomineralized collagen-based tissues (*35*), may be attributed to the cross-linking of HPAA, which acts as cohesive/adhesive "binders" for the collagen/mineral composite hybrid. Similar to cross-linked osteopontin found in the bone (*36*), the bound HPAA may provide a binding layer between the intrafibrillarly mineralized collagen and

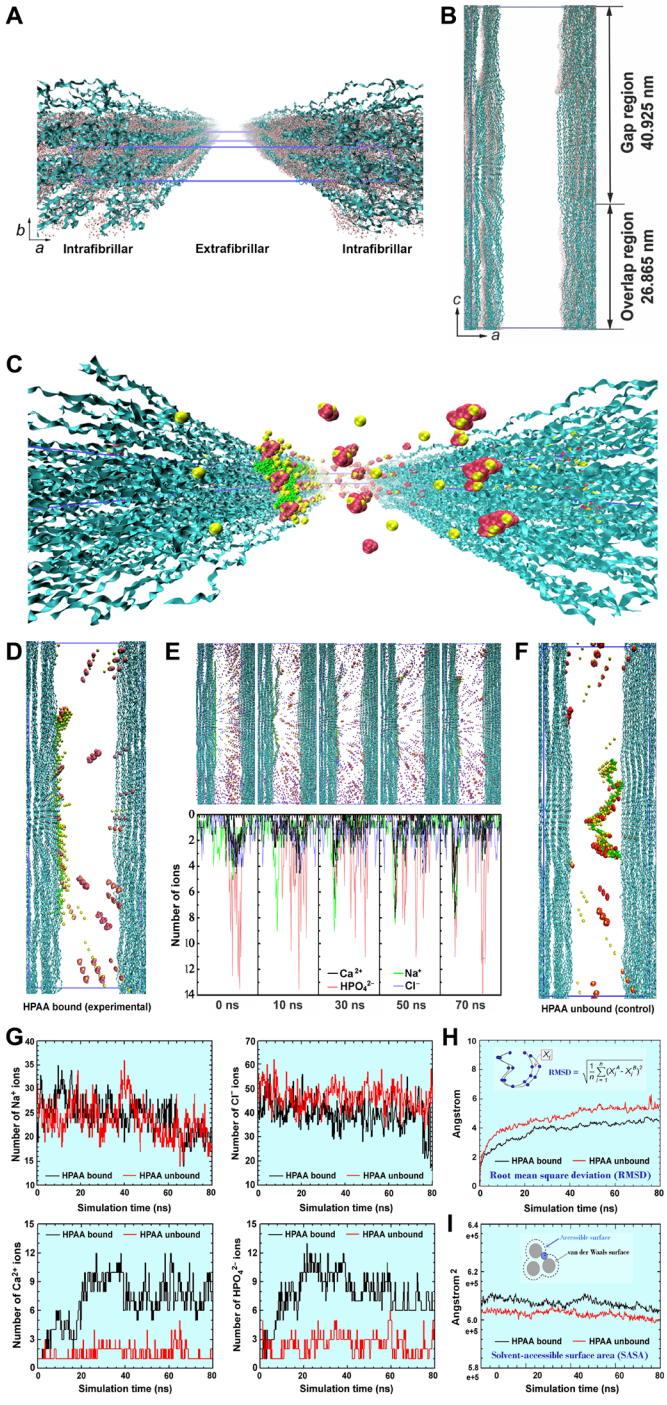

Fig. 3. Molecular dynamics simulations. (**A**) Profile of bare collagen microfibrillar structures with water molecules within the intrafibrillar spaces. Blue ribbons, collagen triple helices; red dots, water molecules. (**B**) Side view of bare collagen microfibrils. The blue lines describe the 67-nm-long simulation box; the dimensions of which are a = 24.2 nm, b = 2.83 nm, and c = 67.79 nm with $\alpha = 90°$, $\beta = 90°$, and $\gamma = 105.58°$. (**C** and **D**) Movement of Ca^{2+} (yellow spheres), HPO_4^{2-} (red assemblies), and assembled CaP mineralization precursors (yellow-red assemblies) across the collagen microfibrils with the HPAA (green chain) bound to the LYS1099 amino acids of the collagen molecules. Water molecules, Na^+, and Cl^- ions are not shown for clearer viewing. (**E**) Top: Simulation of the movement of various ions across the HPAA-collagen microfibrillar structures at designated simulation times. Blue spheres, purple spheres, yellow spheres, red assembly, yellow-red assemblies, and green chain structure represent Na^+ ions, Cl^- ions, Ca^{2+} ions, HPO_4^{2-} ions, CaP mineralization precursors, and HPAA, respectively. Bottom: Dynamic changes in the number of Ca^{2+} (black line), HPO_4^{2-} (red line), Na^+ (green line), and Cl^- (blue line) in the intrafibrillar and extrafibrillar regions along the a-axis boundary at 0, 30, 50, and 70 ns. (**F**) Movement of Ca^{2+}, HPO_4^{2-}, and assembled CaP mineralization precursors across the bare collagen microfibrils with unbound HPAA in the extrafibrillar region (control). (**G**) Comparison of the distribution of various ions within the intrafibrillar region in the collagen-bound HPAA and the unbound HPAA mineralization models. (**H**) Comparison of root mean square deviation of collagen molecules in the collagen-bound HPAA and the unbound HPAA models. (**I**) Comparison of solvent-accessible surface area (SASA) of the collagen molecules between the two models.

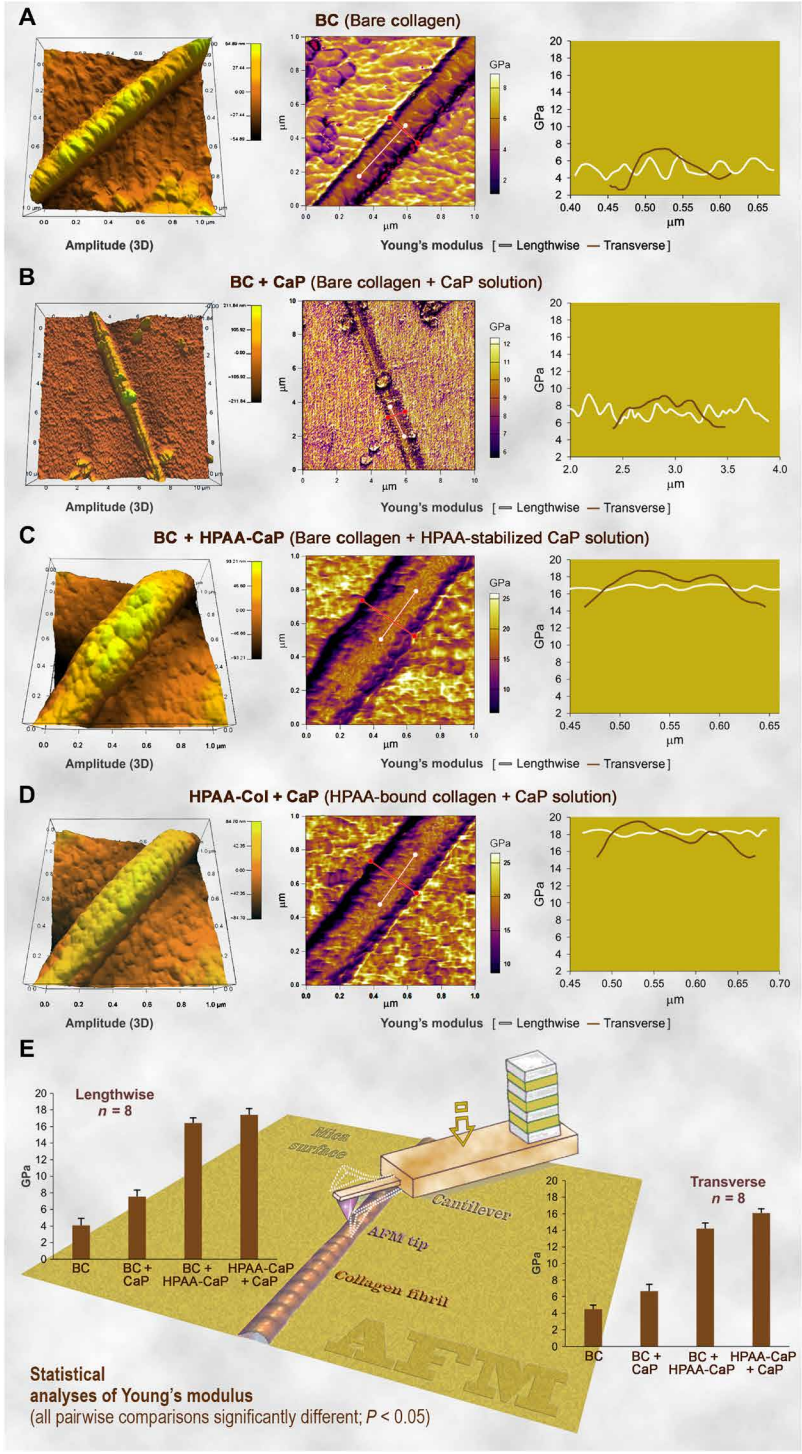

Fig. 4. AFM of the 3D surface topography and modulus of elasticity (Young's modulus) mapping of representative air-dried, mineralized bare collagen and HPAA-collagen fibrils. (**A**) Bare collagen fibrils (BC) had a close-to-normal distribution of Young's modulus transversely across the fibril. A sinusoidal pattern of variation in Young's modulus was detected lengthwise along the fibril, corresponding to the periodic topographic variations along the fibril's longitudinal axis. (**B**) Bare collagen mineralized in CaP solution without nucleation inhibitor (BC + CaP). The transverse Young's modulus of the CaP group was similar to the BC group. Periodic variation in the lengthwise Young's modulus was not obvious, which may be attributed to the random deposition of extrafibrillar minerals on the fibril's surface. (**C**) Bare collagen mineralized with HPAA-CaP solution (BC + HPAA-CaP). After intrafibrillar mineralization, both the transverse and lengthwise Young's moduli of the collagen fibril were significantly increased. (**D**) HPAA-collagen mineralized with CaP solution without nucleation inhibitor (HPAA-Col + CaP). Features were similar to the BC + HPAA-CaP group. (**E**) Statistical analyses of the Young's modulus of collagen fibril in the lengthwise and transverse directions ($n = 8$). For each chart, pairwise comparisons of the differences among the four groups were all significantly different ($P < 0.05$). Schematic in the background depicts how mapping of a collagen fibril was performed using an AFM tip.

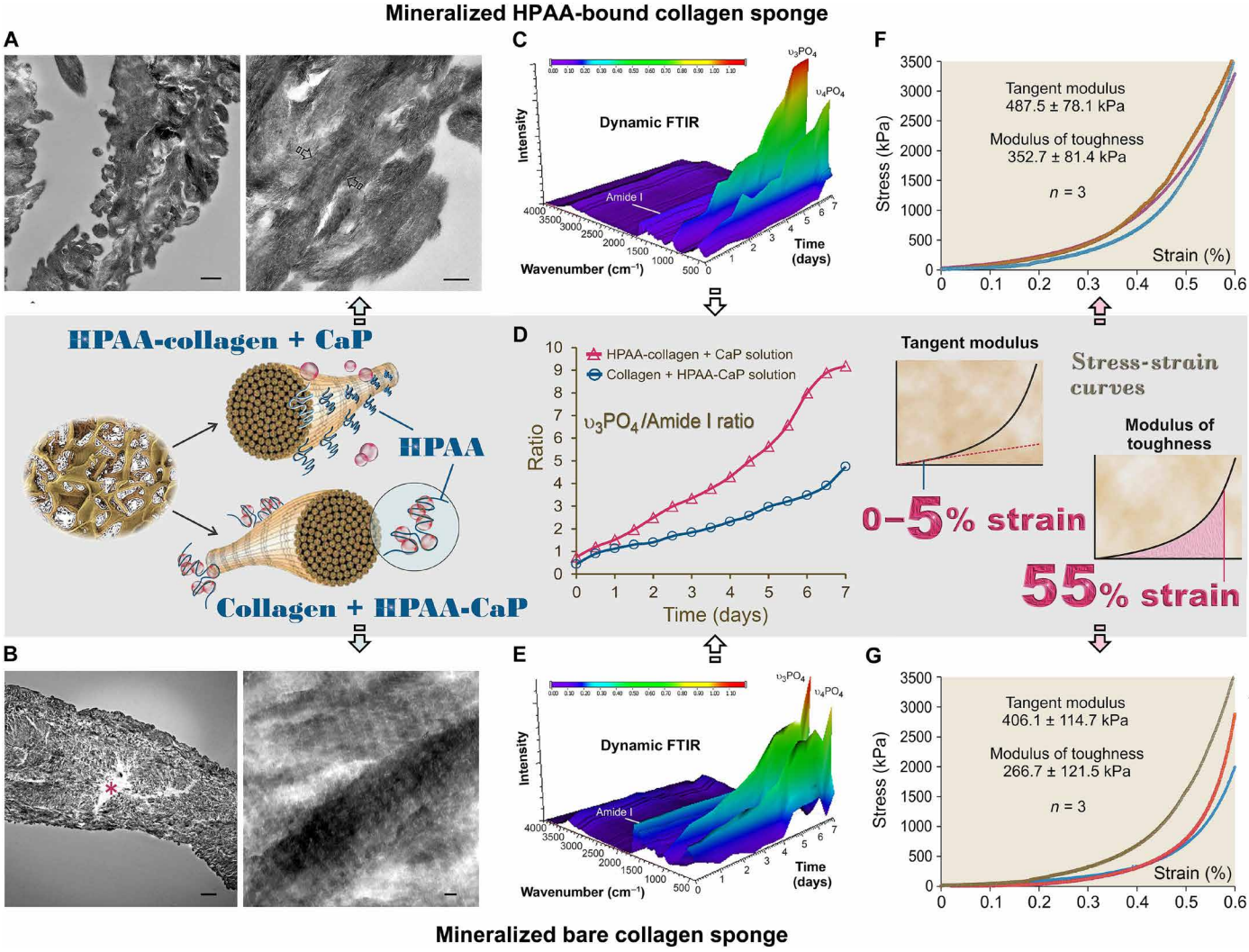

Fig. 5. Characterization of mineralized HPAA-collagen sponges and bare collagen sponges. (**A**) TEM of mineralized HPAA-collagen sponges. Left: Dense mineralization in collagen leaflets cross-linked with HPAA and immersed in CaP solution for 7 days (left inset, middle row). Scale bar, 500 nm. Right: Collagen fibrils within leaflet were filled with apatite crystallites oriented along the longitudinal axis of the fibril (between open arrows). Scale bar, 200 nm. (**B**) TEM of mineralized bare collagen sponges. Left: Heavily mineralized collagen leaflet after immersion in HPAA-CaP solution for 7 days. Nevertheless, the central part of the leaflet was not mineralized (asterisk). Scale bar, 2 μm. Right: Intrafibrillar apatite crystallites arranged along the longitudinal axis of the fibrils. Scale bar, 50 nm. (**C**) Dynamic attenuated total reflection (ATR)–FTIR shows progressive mineralization of an HPAA-collagen sponge at 12-hour intervals over a 7-day period. Spectra were normalized along the collagen amide I peak (~1640 cm^{-1}). (**D**) Changes in apatite υ_3PO_4/collagen amide I ratio of mineralized anionic collagen sponges and unmodified collagen sponges. Compared to bare collagen sponges mineralized in HPAA-CaP solution, HPAA-collagen sponges mineralized in CaP solution demonstrated increases in both the mineralization rate (slope of curves) and extent of mineralization. (**E**) Dynamic ATR-FTIR shows the progress of mineralization of a bare collagen sponge in HPAA-CaP solution. (**F**) Stress-strain response of mineralized HPAA-collagen sponges for determining tangent modulus and modulus of toughness (right inset, middle row). (**G**) Stress-strain response of mineralized bare collagen sponges.

the extrafibrillar minerals, which enhances interfacial adhesion and the fracture toughness of the material.

The cross-linked HPAA is likely to be retained on the collagen matrices after mineralization. The biocompatibility of the HPAA–cross-linked collagen is important from a materials science perspective. These matrices should not hamper the survival and proliferation of stem cells recruited for bone regeneration. Mitochondrial dehydrogenase and apoptosis assays performed on human mesenchymal stem cells indicate no significant difference between unmineralized HPAA-collagen and bare collagen sponges (fig. S10). PAA has also been shown to be biocompatible to human osteoblast–like cells when used as coatings for surgical implants (*37*). Because synthetic nucleation inhibitors cannot be replenished in a surgical site to stabilize mineralization precursors, the use of the polyelectrolyte–cross-linked collagen matrices may be a better alternative to bare collagen matrices for tissue-engineering applications.

CONCLUSIONS

The present model of intrafibrillar mineralization enhancement by collagen-ligand interaction provides strong support for future investigations on site-specific intrafibrillar mineralization mechanisms

using, for example, enzymatic cross-linking of osteopontin to collagen (*38*). Because collagen matrices that do not mineralize naturally may be induced to mineralize using nucleation inhibitor–stabilized CaP precursors (*9*, *10*), previously reported mineralization mechanisms that use unbound nucleation inhibitors do not provide the cue for heterogeneously mineralized tissues such as tendon ossification in the avian hind limb. Matrix phosphoproteins were identified in the mineralizable part of the turkey leg tendon and increased in concentration as mineralization proceeded. In contrast, the concentrations of those proteins were minimal or absent in areas of the tendon that did not calcify (*39*). The present model of collagen-ligand interaction also sheds light on the potential causes of ectopic mineralization in the skin, joints, heart valves, and blood vessels as the currently proposed balance between procalcific and anticalcific factors remains to be proven (*17*, *40*). From a materials science perspective, the enhancement of intrafibrillar mineralization by collagen-ligand interaction produces a more consistent infiltration of minerals within bulk collagen matrices, with better mechanical properties and potential flaw reduction to increase fatigue resistance of the mineralized collagen matrix.

MATERIALS AND METHODS

Development and characterization of nucleation inhibitor–bound collagen model

PAA [450 kDa (HPAA) and 2 kDa (LPAA)] was covalently bound to collagen fibrils via 1-ethyl-3-(3-dimethylaminopropyl)-carbodiimide (EDC)/*N*-hydroxysulfosuccinimide sodium salt (sulfo-NHS) cross-linking. Briefly, 125 mg of HPAA or LPAA was dissolved in 25 ml of 0.1 M MES buffer (pH 6.0) and mixed with 10 mg of EDC and 27.5 mg of sulpho-NHS for 15 min for NHS-ester activation. The pH of the mixture was increased to 7.3 using concentrated phosphate-buffered saline [0.1 M sodium phosphate and 0.15 M NaCl (pH 7.2 to 7.5)]. Collagen sponges (bovine type I collagen, ACE Surgical Supply Co. Inc., Brockton, MA, USA) or TEM grids containing a single layer of reconstituted collagen on their surfaces were incubated with the solution for 30 min at room temperature. The collagen was washed six times with Milli-Q water (18.2 megaohms) for 10 min, lyophilized, and used as the nucleation inhibitor–bound collagen model. For the bare collagen control, the cross-linking of the collagen was performed using EDC/sulfo-NHS only, without PAA. The PAA-collagen was then characterized with a series of chemo/physio-analytical methods (Supplementary Materials and Methods).

Mineralization of the nucleation inhibitor–bound collagen

Preparation of the mineralization medium

CaP mineralization medium was prepared by mixing 50 ml of 9 mM $CaCl_2{\cdot}2H_2O$ with an equal volume of 4.2 mM K_2HPO_4. To maintain the pH of the mineralization solutions at 7.4, the two solutions were prepared using 10 mM Hepes buffer with 150 mM NaCl. For the preparation of nucleation inhibitor–stabilized CaP solutions (HPAA-CaP), HPAA was added to the supersaturated CaP mineralization medium at a concentration of 50 μg/ml. The particle size distribution, ζ potential, and ultrastructure of the particles in the mineralization medium were then examined.

Cryo-EM electron tomography

A single layer of collagen was reconstituted on QUANTIFOIL Jena R 2/2 gold grids (holey carbon support film with 2-μm holes) and cross-linked with EDC/sulfo-NHS only (control) or with HPAA, using EDC/sulfo-NHS as the cross-linking agent. Control grids with bare collagen were incubated in HPAA-CaP, while grids containing HPAA-collagen were incubated in unstabilized CaP solution for 1 to 72 hours. After retrieving from the mineralization solutions, the grids were vitrified without previous staining and examined with the Talos F200C microscope (Supplementary Materials and Methods).

For electron tomography, grids of interest were imaged by tilting the grid in 2° steps from approximately 60° to −60°. The total electron dosage for the entire tilt series was estimated at ~100 $e/Å^2$ per tilt series. Tomograms were reconstructed using the weighted back-projection method. Segmentation and visualization of the 3D volume were performed using Amira 5.3.3 (Visage Imaging Inc., Andover, MA, USA) and MATLAB R2014a and 3D Volume Visualization package 1.1 (MathWorks Inc., Natick, MA, USA).

Molecular dynamics simulation of the mineralization process

Full atomistic molecular dynamics simulation of a high-resolution HPAA-collagen structure was constructed to investigate the effect of the presence of large polyelectrolyte molecules along the surface of collagen fibril on the movement and infiltration of ions (Supplementary Materials and Methods).

Comparison between the collagen mineralized with two different schemes

The HPAA-collagen mineralized in CaP solution and the bare collagen mineralized in HPAA-CaP solution were examined with TEM, powder x-ray diffraction, and thermogravimetric analysis. The mechanical properties of the mineralized collagen were examined with AFM and compressive stress-strain test. The kinetics of the mineralization processes were characterized with dynamic attenuated total reflection–FTIR (Supplementary Materials and Methods).

Cellular responses of human mesenchymal stem cells (Texas A&M Health Science Center, Institute for Regenerative Medicine, College Station, TX, USA) to bare collagen sponges and HPAA-collagen sponges were evaluated using 3-(4,5-dimethylthiazol-2-yl)-2,5-diphenyltetrazolium bromide assay and flow cytometry (Supplementary Materials and Methods).

Statistical analyses

Parametric statistical methods were used after validating the normality and homoscedasticity assumptions of the corresponding datasets. If either of those assumptions was violated, then the data were nonlinearly transformed to satisfy those assumptions before the use of parametric analytical methods. One-factor ANOVA and Holm-Šídák pairwise comparison procedures were used to compare the ζ potential, carboxylic groups, and amine groups among bare collagen, LPAA-collagen, and HPAA-collagen. The same procedures were used to separately compare the lengthwise Young's modulus and transverse Young's modulus of the four groups in the AFM test. Separate Student's *t* tests were used to compare the tangent modulus and the modulus of toughness of the two intrafibrillarly mineralized collagen sponges in the compressive stress-strain test. The same procedures were used to evaluate the effect of materials on the cell viability of the human mesenchymal stem cells. For all analyses, statistical significance was preset at $\alpha = 0.05$.

SUPPLEMENTARY MATERIALS

Supplementary material for this article is available at http://advances.sciencemag.org/cgi/content/full/5/3/eaav9075/DC1

Supplementary Materials and Methods

Fig. S1. Schematic diagram of conjugation of polyanions to bonding of collagen fibrils.

Fig. S2. Snapshot of the simulation of the Ca^{2+}, HPO_4^{2-}, and PAA system.

Fig. S3. Conventional TEM of ruthenium red and uranyl acetate stained collagen fibrils.

Fig. S4. High performance liquid chromatography of HPAA-collagen in various extraction media.

Fig. S5. Particle size distribution of the mineralizing solution.

Fig. S6. Representative TEM images of different mineralization phase of HPAA-collagen.

Fig. S7. Conventional TEM examination of LPAA-collagen mineralized with CaP.

Fig. S8. Molecular dynamics simulation of several collagen fibrillar strctures containing bound HPAA molecules.

Fig. S9. Characterization of mineralized collagen fibrils.

Fig. S10. Biocompatibility evaluation of bare collagen sponges versus HPAA-collagen sponges.

Movie S1. Molecular dynamics simulation of aggregation of Ca^{2+} and HPO_4^{2-} in the presence of PAA.

Movie S2. Early phase of intrafibrillar mineralization of HPAA-collagen.

Movie S3. Middle phase of intrafibrillar mineralization of HPAA-collagen.

Movie S4. Late phase of intrafibrillar mineralization of HPAA-collagen.

REFERENCES AND NOTES

1. H. Ehrlich, R. Deutzmann, E. Brunner, E. Cappellini, H. Koon, C. Solazzo, Y. Yang, D. Ashford, J. Thomas-Oates, M. Lubeck, C. Baessmann, T. Langrock, R. Hoffmann, G. Wörheide, J. Reitner, P. Simon, M. Tsurkan, A. V. Ereskovsky, D. Kurek, V. V. Bazhenov, S. Hunoldt, M. Mertig, D. V. Vyalikh, S. L. Molodtsov, K. Kummer, H. Worch, V. Smetacek, M. J. Collins, Mineralization of the metre-long biosilica structures of glass sponges is templated on hydroxylated collagen. *Nat. Chem.* **2**, 1084–1088 (2010).
2. H. S. Gupta, J. Seto, W. Wagermaier, P. Zaslansky, P. Boesecke, P. Fratzl, Cooperative deformation of mineral and collagen in bone at the nanoscale. *Proc. Natl. Acad. Sci. U.S.A.* **103**, 17741–17746 (2006).
3. A. Veis, J. R. Dorvee, Biomineralization mechanisms: A new paradigm for crystal nucleation in organic matrices. *Calcif. Tissue Int.* **93**, 307–315 (2013).
4. F. Nudelman, A. J. Lausch, N. A. J. M. Sommerdijk, E. D. Sone, In vitro models of collagen biomineralization. *J. Struct. Biol.* **183**, 258–269 (2013).
5. K. Jiao, L.-N. Niu, C.-F. Ma, X.-Q. Huang, D.-D. Pei, T. Luo, Q. Huang, J.-H. Chen, F. R. Tay, Complementarity and uncertainty in intrafibrillar mineralization of collagen. *Adv. Funct. Mater.* **26**, 6858–6875 (2016).
6. W. J. Landis, F. H. Silver, Mineral deposition in the extracellular matrices of vertebrate tissues: Identification of possible apatite nucleation sites on type I collagen. *Cells Tissues Organs* **189**, 20–24 (2008).
7. D. Toroian, J. E. Lim, P. A. Price, The size exclusion characteristics of type I collagen: Implications for the role of noncollagenous bone constituents in mineralization. *J. Biol. Chem.* **282**, 22437–22447 (2007).
8. Y. Wang, T. Azaïs, M. Robin, A. Vallée, C. Catania, P. Legriel, G. Pehau-Arnaudet, F. Babonneau, M.-M. Giraud-Guille, N. Nassif, The predominant role of collagen in the nucleation, growth, structure and orientation of bone apatite. *Nat. Mater.* **11**, 724–733 (2012).
9. L. B. Gower, Biomimetic model systems for investigating the amorphous precursor pathway and its role in biomineralization. *Chem. Rev.* **108**, 4551–4627 (2008).
10. F. Nudelman, K. Pieterse, A. George, P. H. H. Bomans, H. Friedrich, L. J. Brylka, P. A. J. Hilbers, G. de With, N. A. M. Sommerdijk, The role of collagen in bone apatite formation in the presence of hydroxyapatite nucleation inhibitors. *Nat. Mater.* **9**, 1004–1009 (2010).
11. L.-n. Niu, S. E. Jee, K. Jiao, L. Tonggu, M. Li, L. Wang, Y.-d. Yang, J.-h. Bian, L. Breschi, S. S. Jang, J.-h. Chen, D. H. Pashley, F. R. Tay, Collagen intrafibrillar mineralization as a result of the balance between osmotic equilibrium and electroneutrality. *Nat. Mater.* **16**, 370–378 (2017).
12. C. L. Hoop, J. Zhu, A. M. Nunes, D. A. Case, J. Baum, Revealing accessibility of cryptic protein binding sites within the functional collagen fibril. *Biomolecules* **7**, E76 (2017).
13. J. D. Termine, H. K. Kleinman, S. W. Whitson, K. M. Conn, M. L. McGarvey, G. R. Martin, Osteonectin, a bone-specific protein linking mineral to collagen. *Cell* **26**, 99–105 (1981).
14. W. Pompe, H. Worch, W. J. E. M. Habraken, P. Simon, R. Kniep, H. Ehrlichd, P. Pauflere, Octacalcium phosphate—A metastable mineral phase controls the evolution of scaffold forming proteins. *J. Mater. Chem. B* **3**, 5318–5329 (2015).
15. P. Simon, D. Grüner, H. Worch, W. Pompe, H. Lichte, T. El Khassawna, C. Heiss, S. Wenisch, R. Kniep, First evidence of octacalcium phosphate@osteocalcin nanocomplex as skeletal bone component directing collagen triple-helix nanofibril mineralization. *Sci. Rep.* **8**, 13696 (2018).
16. T. Nagata, A. Kawahara, C. Kasahara, M. Yokota, S. Nishikawa, Y. Wakano, H. Ishida, Biochemical study on the tissue compartmentalization of phosphophoryn, osteopontin and bone sialoprotein (BSP) in rat incisor dentin. *J. Bone Miner. Metab.* **12**, 7–13 (1994).
17. Q. Li, Q. Jiang, J. Uitto, Ectopic mineralization disorders of the extracellular matrix of connective tissue: Molecular genetics and pathomechanisms of aberrant calcification. *Matrix Biol.* **33**, 23–28 (2014).
18. G. E. Donley, L. A. Fitzpatrick, Noncollagenous matrix proteins controlling mineralization; possible role in pathologic calcification of vascular tissue. *Trends Cardiovasc. Med.* **8**, 199–206 (1998).
19. T. Saito, A. L. Arsenault, M. Yamauchi, Y. Kuboki, M. A. Crenshaw, Mineral induction by immobilized phosphoproteins. *Bone* **21**, 305–311 (1997).
20. J. G. Kerns, K. Buckley, J. Churchwell, A. W. Parker, P. Matousek, A. E. Goodship, Is the collagen primed for mineralization in specific regions of the turkey tendon? An investigation of the protein-mineral interface using Raman spectroscopy. *Anal. Chem.* **88**, 1559–1563 (2016).
21. N. Clemente, D. Raineri, G. Cappellano, E. Boggio, F. Favero, M. F. Soluri, C. Dianzani, C. Comi, U. Dianzani, A. Chiocchetti, Osteopontin bridging innate and adaptive immunity in autoimmune diseases. *J. Immunol. Res.* **2016**, 7675437 (2016).
22. M. L. Zoch, T. L. Clemens, R. C. Riddle, New insights into the biology of osteocalcin. *Bone* **82**, 42–49 (2016).
23. N. Nakajima, Y. Ikada, Mechanism of amide formation by carbodiimide for bioconjugation in aqueous media. *Bioconjug. Chem.* **6**, 123–130 (1995).
24. A. A. Hyman, C. A. Weber, F. Jülicher, Liquid-liquid phase separation in biology. *Annu. Rev. Cell Dev. Biol.* **30**, 39–58 (2014).
25. G. Mancardi, U. Terranova, N. H. Leeuw, Calcium phosphate prenucleation complexes in water by means of ab initio molecular dynamics simulations. *Cryst. Growth Des.* **16**, 3353–3358 (2016).
26. A. Dey, P. H. H. Bomans, F. A. Müller, J. Will, P. M. Frederik, G. de With, N. A. J. M. Sommerdijk, The role of prenucleation clusters in surface-induced calcium phosphate crystallization. *Nat. Mater.* **9**, 1010–1014 (2010).
27. C. Yigit, J. Heyda, M. Ballauff, J. Dzubiella, Like-charged protein-polyelectrolyte complexation driven by charge patches. *J. Chem. Phys.* **143**, 064905 (2015).
28. F. L. Barroso da Silva, M. Boström, C. Persson, Effect of charge regulation and ion-dipole interactions on the selectivity of protein-nanoparticle binding. *Langmuir* **30**, 4078–4083 (2014).
29. I. Streeter, N. H. de Leeuw, Atomistic modeling of collagen proteins in their fibrillar environment. *J. Phys. Chem. B* **114**, 13263–13270 (2010).
30. L. Bertinetti, A. Masic, R. Schuetz, A. Barbetta, B. Seidt, W. Wagermaier, P. Fratzl, Osmotically driven tensile stress in collagen-based mineralized tissues. *J. Mech. Behav. Biomed. Mater.* **52**, 14–21 (2015).
31. Y. Liu, D. Luo, X.-X. Kou, X.-D. Wang, F. R. Tay, Y.-L. Sha, Y.-H. Gan, Y.-H. Zhou, Hierarchical intrafibrillar nanocarbonated apatite assembly improves the nanomechanics and cytocompatibility of mineralized collagen. *Adv. Funct. Mater.* **23**, 1404–1411 (2013).
32. C. A. Grant, M. A. Phillips, N. H. Thomson, Dynamic mechanical analysis of collagen fibrils at the nanoscale. *J. Mech. Behav. Biomed. Mater.* **5**, 165–170 (2012).
33. E.-C. Spitzner, S. Röper, M. Zerson, A. Bernstein, R. Magerle, Nanoscale swelling heterogeneities in type I collagen fibrils. *ACS Nano* **9**, 5683–5694 (2015).
34. Y. K. Kim, S. Mai, A. Mazzoni, Y. Liu, A. Tezvergil-Mutluay, K. Takahashi, K. Zhang, D. H. Pashley, F. R. Tay, Biomimetic remineralization as a progressive dehydration mechanism of collagen matrices—Implications in the aging of resin-dentin bonds. *Acta Biomater.* **6**, 3729–3739 (2010).
35. J. Schwiedrzik, A. Taylor, D. Casari, U. Wolfram, P. Zysset, J. Michler, Nanoscale deformation mechanisms and yield properties of hydrated bone extracellular matrix. *Acta Biomater.* **60**, 302–314 (2017).
36. S. Cavelier, A. K. Dastjerdi, M. D. McKee, F. Barthelat, Bone toughness at the molecular scale: A model for fracture toughness using crosslinked osteopontin on synthetic and biogenic mineral substrates. *Bone* **110**, 304–311 (2018).
37. E. De Giglio, D. Cafagna, M. A. Ricci, L. Sabbatini, S. Cometa, C. Ferretti, M. Mattioli-Belmonte, Biocompatibility of poly(acrylic acid) thin coatings electro-synthesized onto TiAlV-based implants. *J. Bioact. Compat. Polym.* **25**, 374–391 (2010).
38. M. T. Kaartinen, A. Pirhonen, A. Linnala-Kankkunen, P. H. Mäenpää, Cross-linking of osteopontin by tissue transglutaminase increases its collagen binding properties. *J. Biol. Chem.* **274**, 1729–1735 (1999).
39. M. J. Glimcher, D. Brickley-Parsons, D. Kossiva, Phosphopeptides and γ-carboxyglutamic acid-containing peptides in calcified turkey tendon: Their absence in uncalcified tendon. *Calcif. Tissue Int.* **27**, 281–284 (1979).
40. N. Reznikov, J. A. M. Steele, P. Fratzl, M. M. Stevens, A materials science vision of extracellular matrix mineralization. *Nat. Rev. Mater.* **1**, 16041 (2016).

Acknowledgments: We thank J. Liu, H.-m. Tong, and S. E. Jee for assistance in the TEM examination and molecular dynamics simulations. **Funding:** This work was supported by grants 81722015, 81870805, 81720108011, and 81671012 from National Natural Science Foundation of China and program IRT13051 for Changjiang Scholars and Innovative Research Team in University. **Author contributions:** Q.S. and K.J. performed the mineralization

experiments and analytical part of the study and wrote the manuscript. L.T., L.G.W., S.L.Z., L.Z., and D.X.H. contributed to cryo-TEM examination and the molecular dynamic simulation. J.H.B., C.Y.W., Y.X.M., and Y.D.Y. contributed to the AFM. D.D.A. and L.B. provided advice on the experimental design and edited the manuscript. L.N.N., J.H.C., and F.R.T. supervised the project and wrote the manuscript. All authors discussed the results and revised the manuscript.
Competing interests: The authors declare that they have no competing interests. **Data availability:** All data needed to evaluate the conclusions in the paper are present in the paper and/or the Supplementary Materials. Additional data related to this paper may be requested from the authors.

Submitted 1 November 2018
Accepted 6 February 2019
Published 29 March 2019
10.1126/sciadv.aav9075

Citation: Q. Song, K. Jiao, L. Tonggu, L. G. Wang, S. L. Zhang, Y. D. Yang, L. Zhang, J. H. Bian, D. X. Hao, C. Y. Wang, Y. X. Ma, D. D. Arola, L. Breschi, J. H. Chen, F. R. Tay, L. N. Niu, Contribution of biomimetic collagen-ligand interaction to intrafibrillar mineralization. *Sci. Adv.* **5**, eaav9075 (2019).